Behaviors of NIH-3T3 Fibroblasts on Graphene/Carbon Nanotubes: Proliferation, Focal Adhesion, and Gene Transfection Studies

Soo-Ryoon Ryoo, Young-Kwan Kim, Mi-Hee Kim, and Dal-Hee Min*

Department of Chemistry, Institute for the BioCentury, Korea Advanced Institute of Science and Technology (KAIST), 373-1 Guseong-dong, Yuseong-gu, Daejeon 305-701, Korea

ABSTRACT Carbon-based materials, including graphene and carbon nanotubes, have been considered attractive candidates for biomedical applications such as scaffolds in tissue engineering, substrates for stem cell differentiation, and components of implant devices. Despite the potential biomedical applications of these materials, only limited information is available regarding the cellular events, including cell viability, adhesion, and spreading, that occur when mammalian cells interface with carbon-based nanomaterials. Here, we report behaviors of mammalian cells, specifically NIH-3T3 fibroblast cells, grown on supported thin films of graphene and carbon nanotubes to investigate biocompatibility of the artificial surface. Proliferation assay, cell shape analysis, focal adhesion study, and quantitative measurements of cell adhesion-related gene expression levels by RT-PCR reveal that the fibroblast cells grow well, with different numbers and sizes of focal adhesions, on graphene- and carbon nanotube-coated substrates. Interestingly, the gene transfection efficiency of cells grown on the substrates was improved up to 250% that of cells grown on a cover glass. The present study suggests that these nanomaterials hold high potential for bioapplications showing high biocompatibility, especially as surface coating materials for implants, without inducing notable deleterious effects while enhancing some cellular functions (*i.e.*, gene transfection and expression).

KEYWORDS: biocompatibility · carbon nanotubes · cell adhesion · gene transfection · graphene

Various nanomaterials with unique physical and chemical properties have been used in the biomedical field,[1] with applications for biosensors,[2] biochips,[3] diagnostic devices,[4] implantable medical devices (*e.g.*, prostheses),[5] drug delivery systems,[6] and imaging probes.[7] In particular, carbon-based nanomaterials (*e.g.*, single/multiwalled carbon nanotubes and graphene) have attracted attention owing to their unique properties such as high conductivity, transparency, mechanical strength, and good tribological characteristics. Especially, graphene[8] has recently been considered as a promising candidate for the fabrication of ultrafast nanoelectronic devices,[9] quantum computers,[10] transparent electrodes,[11] and nanocomposite materials[12] due to its characteristic thermal and mechanical properties and electrical conductivity. In addition, carbon nanotubes and graphenes are currently being used in engineered tissues,[13] implants,[14] diagnostic tools and chips,[15,16] biological imaging,[17] drug delivery carriers,[18] and antibacterial materials.[19] Nevertheless, few detailed studies and quantitative analyses of cell adhesion, spreading, and behavior on carbon-based nanomaterial-coated substrates have been performed to date.

Biocompatibility is an important issue in the development of new nanomaterials for bioapplications. It is of great importance to evaluate cytotoxicities of nanomaterials and to document the information as a database for references. In addition, a fundamental understanding of the interaction of biosystems with nanomaterials at molecular levels, including the induced cellular responses and their effects on the biosystem, is needed. Furthermore, a systematic investigation of the governing factors and properties of the nanomaterials may allow faster and smarter exploitation of their distinct characteristics for bioapplications. The interaction between mammalian cells and artificial substrates is of particular interest. Anchorage-dependent cells require good adhesion to a substrate in order to spread, proliferate, and maintain cellular functions.[20] The cells communicate with the environment through cell surface interactions with the substrate, including the formation of focal adhesions *via* the clustering of integrin receptors.[21] The wettability, chemical composition, stiffness, dimensions, and topographical properties of substrates can affect cell adhesion and consequently cell growth.[22−26]

*Address correspondence to dalheemin@kaist.ac.kr.

Received for review July 29, 2010 and accepted October 15, 2010.

Published online October 27, 2010.
10.1021/nn1018279

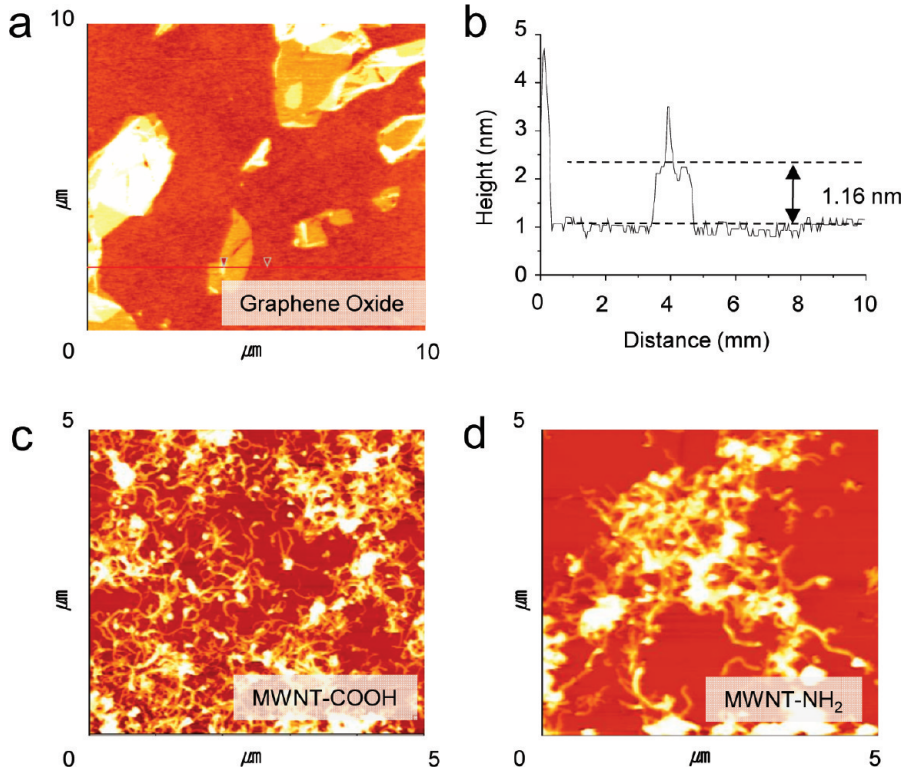

Figure 1. Characterization of the carbon-based nanomaterials: AFM (atomic force microscopic) image (a) and line profile (b) of the exfoliated graphene oxide (GO) sheet showed single-layered structures, about 1 nm in thickness, with solvent evaporation induced aggregated and stacked structures. This result indicates that exfoliated graphene oxide sheets were successfully prepared. The AFM images of multiwalled carbon nanotube (MWNT) functionalized with carboxyl (c) and amine groups (d) confirmed that the physical shape and size of MWNTs were not significantly changed after MWNT surface functionalization.

In this study, NIH-3T3 mouse fibroblasts were used to investigate mammalian cell adhesion, spreading, proliferation, and gene transfection on the carbon nanomaterial-coated substrates. Glass coverslips coated with a thin film of graphene and/or multiwalled carbon nanotubes (MWNTs) were prepared as substrates for adherent cell culture. NIH-3T3 cells were chosen because their adhesive properties (integrin expression pattern, focal adhesion assembly, and spreading) have been well studied previously.[27] They also have been frequently used in studies of cell functions such as cell shape change, adhesion, movement, and proliferation and to demonstrate the key roles of cytoskeletal components in cell adhesion, division, and growth.[28] The present study was designed to investigate the events and cellular responses that occur when cells come into contact with carbon nanomaterial-coated surfaces[29] and to demonstrate the usefulness of these substrates for studies in cell biology.

RESULTS AND DISCUSSION

In this work, glass coverslips were coated with these carbon-based nanomaterials to prepare five different substrates: (i) MWNT, (ii) GO, (iii) a double layer of GO and aminated MWNTs (GO/MWNT), (iv) reduced graphene oxide (RGO), and (v) a double layer of RGO and aminated MWNTs (RGO/MWNT). This allowed us to study each material alone as well as to look for synergistic effects between two carbon nanomaterials. Previously, our group reported the detailed preparation procedures for and characterization of carbon nanomaterial-coated substrates and investigated their application as a large-area transparent electrode.[30] In the present study, we prepared graphene oxide (GO) and aminated MWNTs according to the previously reported methods and analyzed both by atomic force microscopy, scanning electron microscopy (SEM), Raman spectroscopy, UV−vis spectroscopy, dynamic light scattering, and zeta potential analysis (Figure 1; Supporting Information Figure S1). We found that single layers of graphene oxide sheet were prepared with about 1 nm thickness, indicating that the GO sheets were successfully exfoliated. Also, we confirmed that the dimensions of MWNTs were not changed after chemical treatment for surface functionalization (Figure 1).

The MWNT-coated substrate was prepared by immersing a clean glass coverslip presenting epoxy groups in a suspension of aminated MWNT, which resulted in the covalent immobilization of the MWNTs *via* chemical conjugation between the epoxy and amine groups. To make thin films of GO as a substrate, piranha-treated glass was modified with amine groups by using 3-aminopropyltriethoxysilane, and GO sheets were electrostatically adsorbed onto the glass surface.

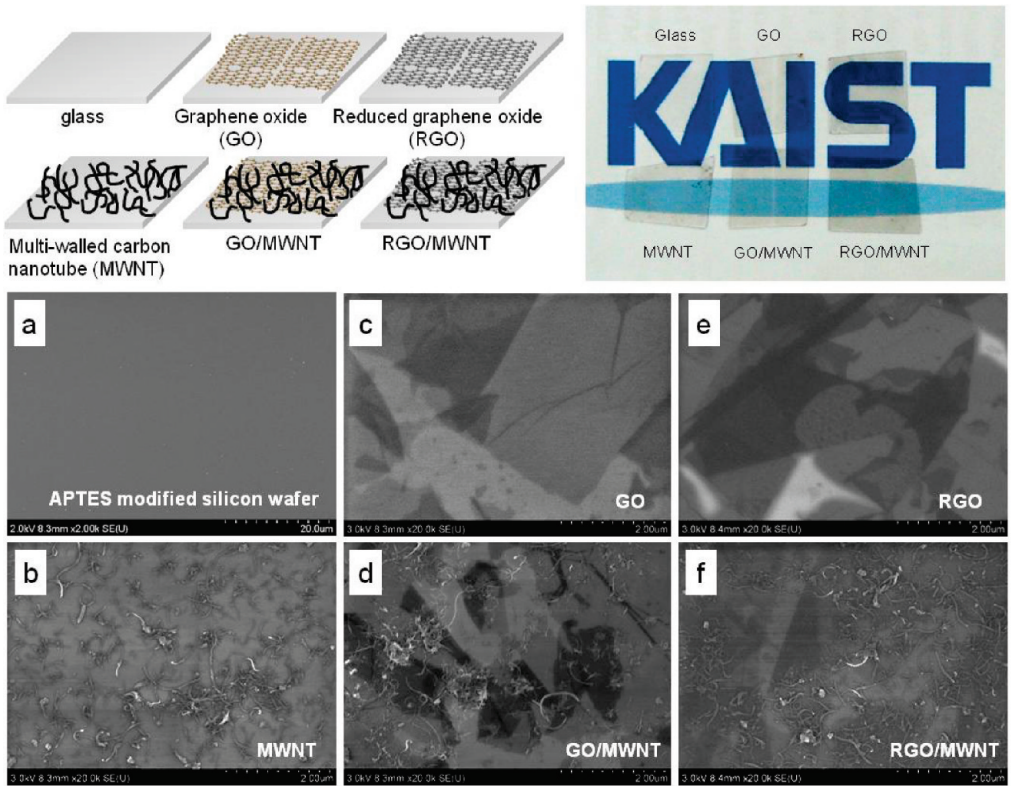

Figure 2. Structural diagrams of GO, RGO, and/or MWNT thin films on the substrate (top left). Optical images of substrates modified with carbon-based nanomaterials. We found that the GO, RGO, MWNT, GO/MWNT, and RGO/MWNT thin films were uniformly immobilized on the glass substrates with high transparency (top right). SEM images show the uniformity and high-density immobilization of MWNT (b), GO sheets (c), and GO/MWNT double layer (d) on silicon substrate. Chemical reduction of GO (e) and GO/MWNT double-layer (f) films did not significantly alter their surface morphologies.

The GO/MWNT substrate was fabricated by submerging a GO-coated glass coverslip in a suspension of aminated MWNTs. The RGO and RGO/MWNT substrates were produced by treating the GO- and GO/MWNT-coated substrates with a reducing agent, hydrazine, for 24 h at 80 °C.

The carbon-based nanomaterials immobilized on a silicon substrate were examined by SEM (Figure 2). For the GO-containing substrates, the entire surface was covered with GO, at an average thickness of 1.16 nm. The surface coverage with MWNTs was not as complete as that with GO, but when deposited on the GO thin films, the MWNTs appeared to be homogeneously distributed. The hydrazine-induced chemical reduction did not alter the morphology or surface coverage of the immobilized materials (Figure 2).

Next, the viability of NIH-3T3 cells after incubation on each substrate for 24 and 48 h was evaluated using live/dead staining with calcein-AM (to stain live cells with green color) and ethidium homodimer (to stain dead cells with red color). Fluorescence microscopy revealed that most of the cells plated on each substrate were alive, and the viabilities were similar to that on sterile glass, which was used as a control (Figure 3a). The proliferation rates, which were calculated by counting the number of live cells per unit area on each substrate, were very similar among the different substrates, with a slightly higher value for the RGO/MWNT-coated substrate (Figure 3b). The cell viability and proliferation assay indicated that all of the prepared substrates may be considered cell-friendly and biocompatible. Ponsonnet[31] and her colleague reported that not only the physicochemical parameters like wettability and surface free energy but also surface roughness influence cell behavior (*e.g.*, cell growth). In the present study, the cell viability on each substrate was not greatly affected by surface hydrophobicity or surface roughness of the substrates immobilized with carbon nanomaterials presumably because the hydrophobicity (measured as water contact angles, 39, 70, 45, 51, 79, and 71° for glass, MWNT, GO, GO/MWNT, RGO, and RGO/MWNT, respectively) and surface roughness of the substrates (0.11, 8.23, 0.701, 2.576, 0.43, and 2.452 nm for glass, MWNT, GO, GO/MWNT, RGO, and RGO/MWNT, respectively) do not cover wide ranges of values enough to induce big differences in cell viability (Supporting Information Figures S2 and S3).

To examine cell adhesion and spreading patterns, NIH-3T3 cells were plated onto each substrate, incubated for 24 and 48 h, and then stained simultaneously with TRITC-conjugated phalloidin to reveal the actin filament network and antivinculin antibody to detect vinculin at focal adhesions[32] (Figure 4). Fluorescence images revealed similar patterns of actin distribution in

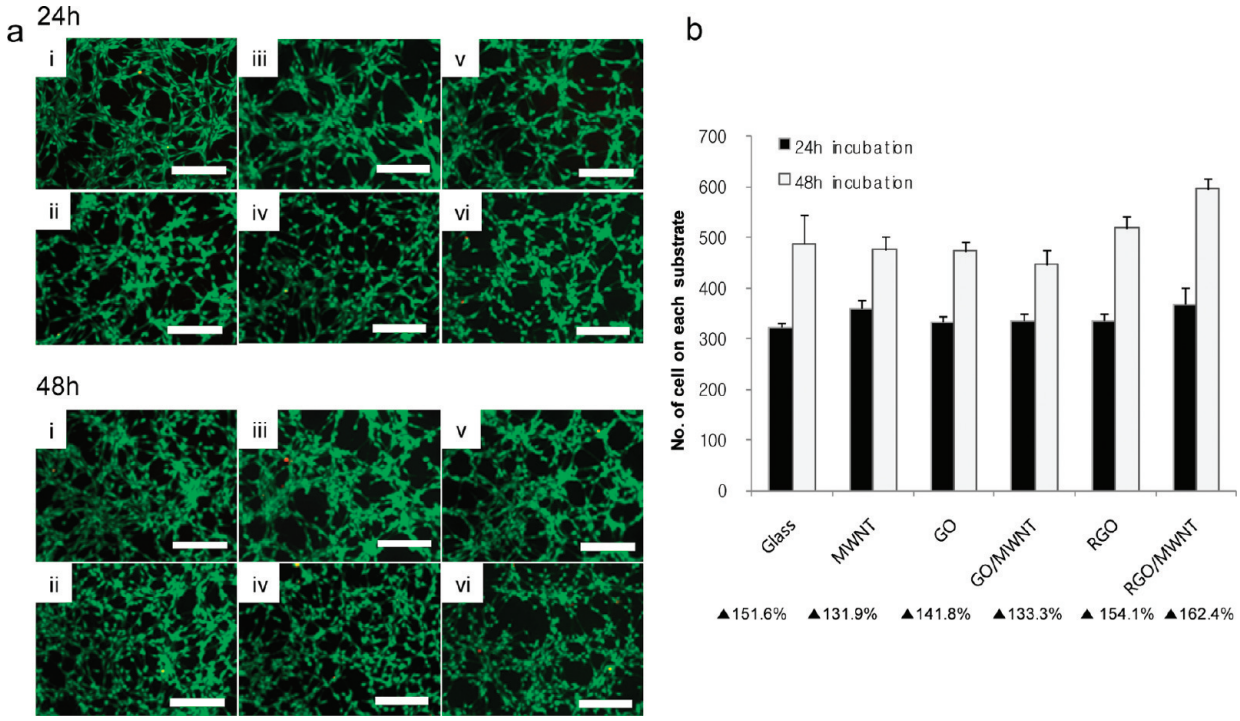

Figure 3. Cell viability is measured by live/dead staining of NIH-3T3 cells after incubation on each substrate for 24 and 48 h (a). Live cells are stained fluorescent green, and dead cells appear red. Substrates: (i) glass; (ii) MWNT; (iii) GO; (iv) GO/MWNT; (v) RGO; and (vi) RGO/MWNT. Numbers of live cells and dead cells were counted and plotted in Supporting Information Figure S4. For the proliferation assay, the number of cells on each substrate was evaluated at 24 and 48 h, and the percentage increase was calculated (b). Scale bars: 100 μm.

NIH-3T3 cells incubated on all of the substrates, including the control glass. However, the vinculin distribution in cells was obviously different between cells cultured on nanomaterial-coated substrates and cells cultured on bare glass. Cells cultured on bare sterile glass exhibited large dot-shaped plaques of vinculin, mainly at the periphery of the cells, whereas smaller vinculin-containing focal contacts were localized at the ventral and peripheral regions of cells cultured on the nanomaterial-coated substrates.

Next, we quantitatively analyzed parameters related to cell morphology, including area of cell spreading, cell shape index (CSI), nuclear shape index (NSI), and number and size of focal adhesions. The cell area was slightly wider on the nanomaterial-coated substrates than on sterile glass (Figure 5a). However, with increased incubation time, the cell area equalized between the modified and sterile glass substrates. After 48 h of incubation, the cell area tended to be a bit broader on substrates containing MWNT (MWNT only, GO/MWNT, and RGO/MWNT) compared with the GO and RGO substrates. This may be attributable to the nanoscopically rougher top surface of the MWNT-containing substrates.

To quantitate and compare cell morphology, the cell and nuclear shape indexes (CSI and NSI) were calculated as the ratio between the cell (or nucleus) length and width. The shape index, which reflects the circularity of an object, can have a value between 0, which indicates a linear shape, and 1, which denotes a circle. The CSI and NSI have been shown to be correlated with various cellular events and functions such as adhesion, spreading, proliferation, and gene expression.[33] For example, Thomas *et al.* reported that the synthesis of collagen I was directly correlated with cell shape and the NSI, such that intermediate values of nuclear distension promoted maximum synthesis of collagen I.[34] The CSIs were similar for NIH-3T3 cells on all of the fabricated substrates, ranging from 0.15 to 0.4, and indicated the elongated morphology characteristic of NIH-3T3 cells (Figure 5b). The cell shapes on the GO and GO/MWNT substrates were slightly more extended after 24 h, but the CSIs were similar to the others after 48 h of incubation. The NSIs were nearly the same, ranging from 0.6 to 0.8, for cells on all of the substrates (Figure 5c). This morphological analysis suggests that carbon-based nanomaterial-coated substrates are not deleterious to cells with respect to adhesion and spreading.

We next analyzed the sizes and the numbers of the focal adhesions per cell. Focal adhesions are dynamic complexes composed of several proteins involved in cellular signaling cascades.[35] The focal adhesion complex serves as a connector between actin filaments and integrins, which bind to the extracellular matrix (ECM). The regulation of focal adhesion assembly is important for integrating many physical cues for cell survival and function, for example, ECM modification, intracellular tension, and cytoskeletal architecture.[36] In addition, the

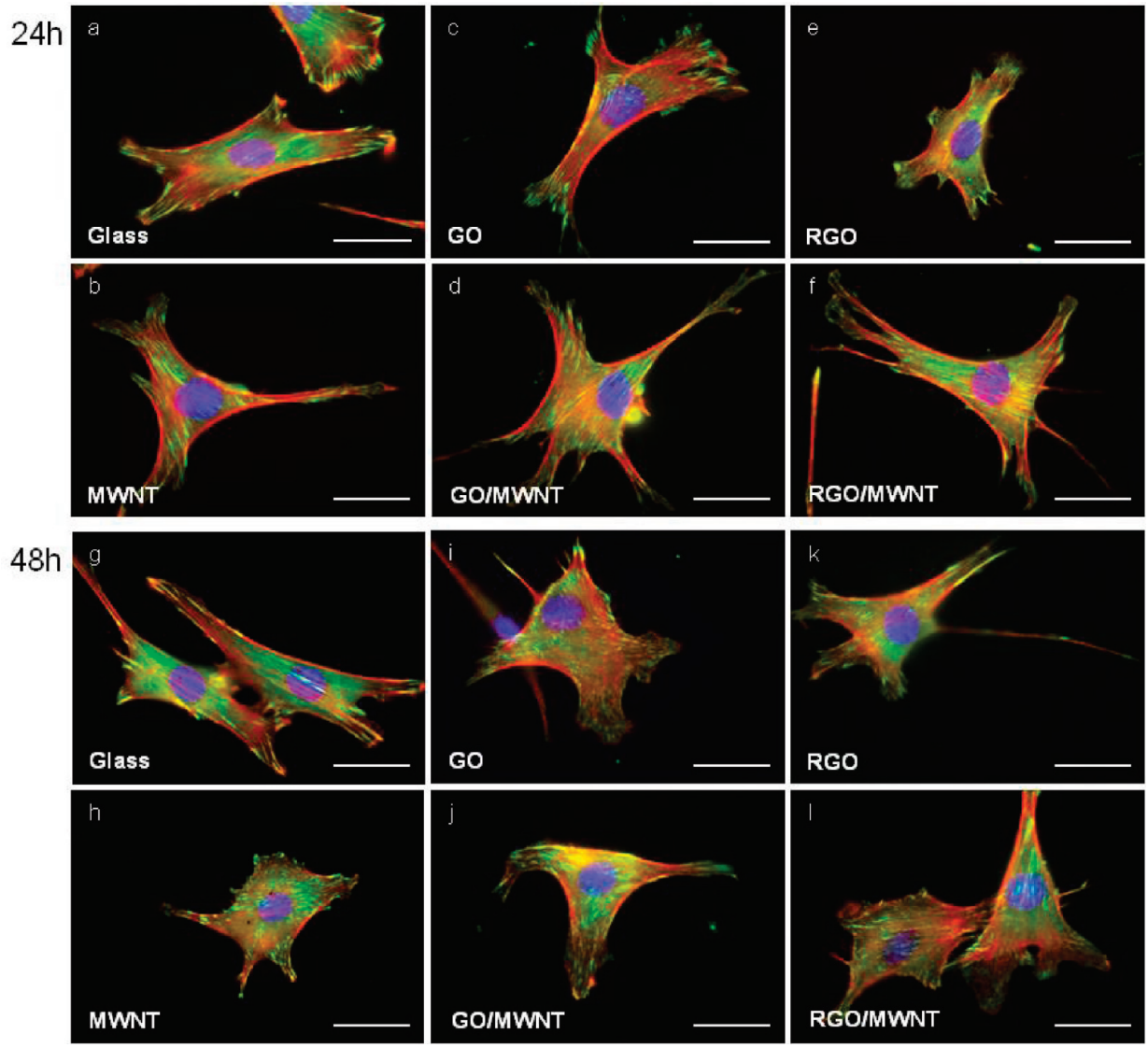

Figure 4. Cell adhesion patterns on various substrates. NIH-3T3 cells were incubated on each substrate for 24 and 48 h, and then actin and vinculin were stained with phalloidin-TRITC and a monoclonal antivinculin antibody, respectively. The merged images depict actin (red), vinculin (green), and the DAPI-stained nucleus (blue). Scale bars: 20 μm.

number of focal adhesions is related to the affinity of cells for a substrate, as it was previously reported that stronger cell−substrate interactions lead to the development of more focal adhesion sites.[37] In the present study, the focal adhesions of cells cultured on glass were generally larger and fewer per cell than those of cells cultured on the carbon-based nanomaterial-coated substrates (Figure 5d,e). These results imply that the cells might have higher affinity for the carbon-based nanomaterials than for bare glass. Cells on the MWNT, GO, and GO/MWNT substrates showed a similar number of focal adhesions per cell, whereas cells cultured on the RGO and RGO/MWNT substrates had fewer focal adhesions per cell but still more than for the cells cultured on glass. The focal adhesion area per focal contact point for cells cultured on sterile glass was significantly larger than that for cells cultured on the substrates of carbon-based nanomaterials (Figure 5f). In addition, we observed that it was more difficult to detach cells grown on the carbon nanomaterial-coated substrates than those on bare glass either through trypsin treatment or mechanical agitation (data not shown). Overall, cells attached strongly to the substrates coated with carbon nanomaterials and developed more focal adhesions with smaller areas, compared with cells on bare glass.

Next, to measure differences in gene expression, the expression levels of adhesion-associated genes, including integrin, focal adhesion kinase, type I collagen (Col I), type III collagen (Col III), and α-actin, and of genes for focal adhesion components such as talin and vinculin were measured by reverse transcription-polymerase chain reaction (RT-PCR). This analytical method is used to measure mRNA levels, though the method provides rough estimates of relative gene expression levels rather than quantitative data. Integrins

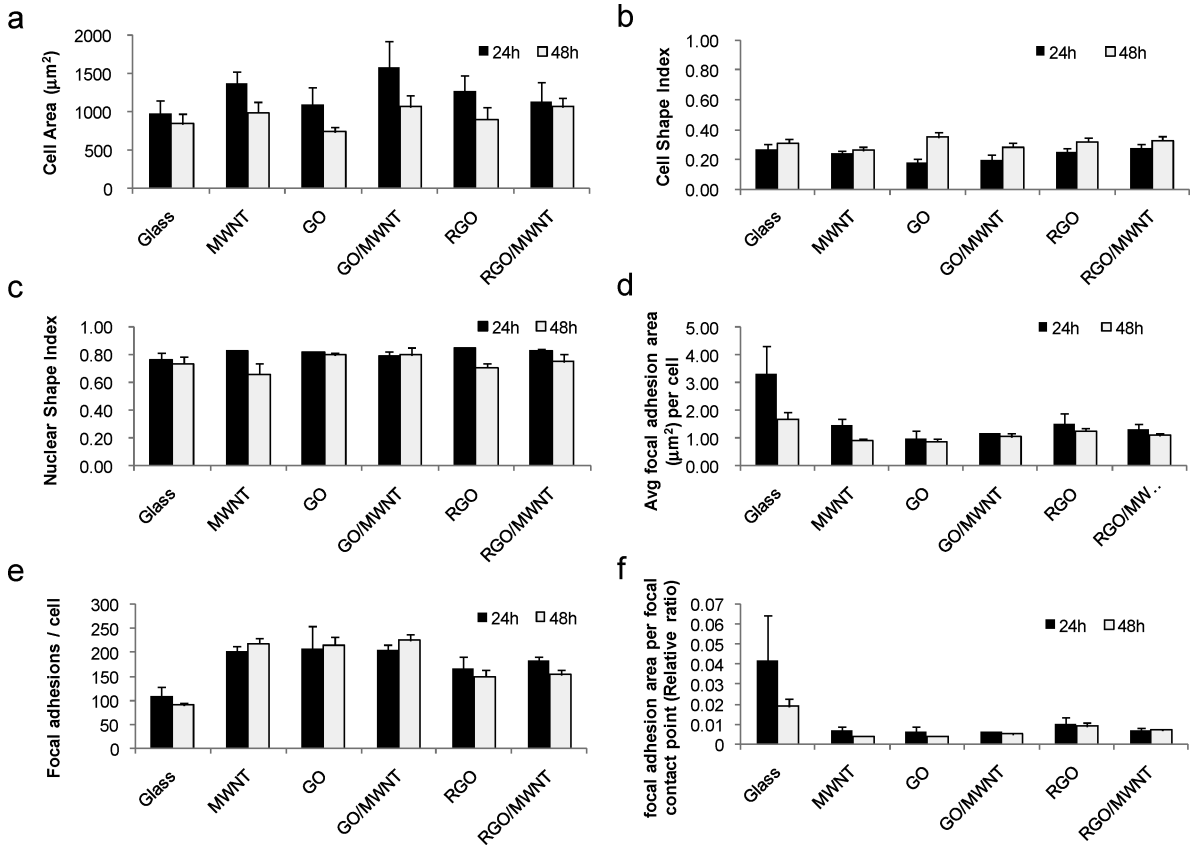

Figure 5. Quantitative analysis of cell adherence to the carbon-based nanomaterial-coated substrates: cell area (a), cell shape index (b), nuclear shape index (c), average focal adhesion area per cell (d), average focal adhesion number per cell (e), and focal adhesion area per contact point (f).

are receptors that engage the attachment between cells and their surrounding tissues (*e.g.*, other cells or ECM) and function in cell migration and invasion by regulating intracellular signaling.[38] Focal adhesion kinase is important in regulating downstream signaling of integrins and growth factor receptors and in regulating integrin-dependent signaling for cell survival.[39] Collagen type I is the predominant collagen and maintains cellular integrity by providing mechanical strength. Collagen type III is also abundant in human tissues, especially tissues having elastic properties, such as blood vessels and skin, and shows increased expression during the granulation stage of wound healing. As a major component of the contractile machinery in vertebrates, α-actin functions in cell movement and shape change. In NIH-3T3 cells grown for 24 and 48 h on each substrate, the expression levels of α-actin, integrin, focal adhesion kinase, Col I, and Col III were similar to each other and among the substrates, whereas talin and vinculin showed more variable expression on the different substrates (Figure 6). Components such as vinculin and talin that are recruited for focal adhesion assembly strengthen the coupling between integrin and the cytoskeleton and initiate the formation of basic nanocomplex clusters. Vinculin, a membrane cytoskeletal protein found in focal adhesion plaques, interacts directly with talin, leading to the clustering of activated integrin[32] and functionally links focal adhesions to the actin cytoskeleton.[40] Both vinculin and talin are involved in the adhesion strengthening response. NIH-3T3 cells cultured on the nanomaterial-coated substrates for 24 h showed increased expression levels of vinculin and talin, compared with cells on the control substrate, with one exception: cells grown on RGO/MWNT showed significantly lower expression levels of vinculin and talin. However, after 48 h of incubation, the expression levels of talin and vinculin were similar among the cells cultured on different substrates. Interestingly, at 48 h, vinculin expression was higher than talin expression in cells on all of the modified substrates except MWNTs. The degree of cell contact has been reported to be regulated by changes in cell density and substrate adhesiveness. Therefore, differences in vinculin expression might have been related to differences in cell−substrate adhesiveness.[41,42] Vinculin expression would be expected to show a relatively dramatic change compared with talin expression within the first 24 h of incubation because of its involvement in the initial contact between cells and the extracellular matrix *via* its many binding domains for cytoskeletal proteins such as actin, α-actin, talin, paxillin, ponsin, vinexin, and protein kinase C. Albigès-Rizo *et al.* showed that a reduction in talin expression dramatically slowed the kinetics of cell spreading and that cells with reduced talin

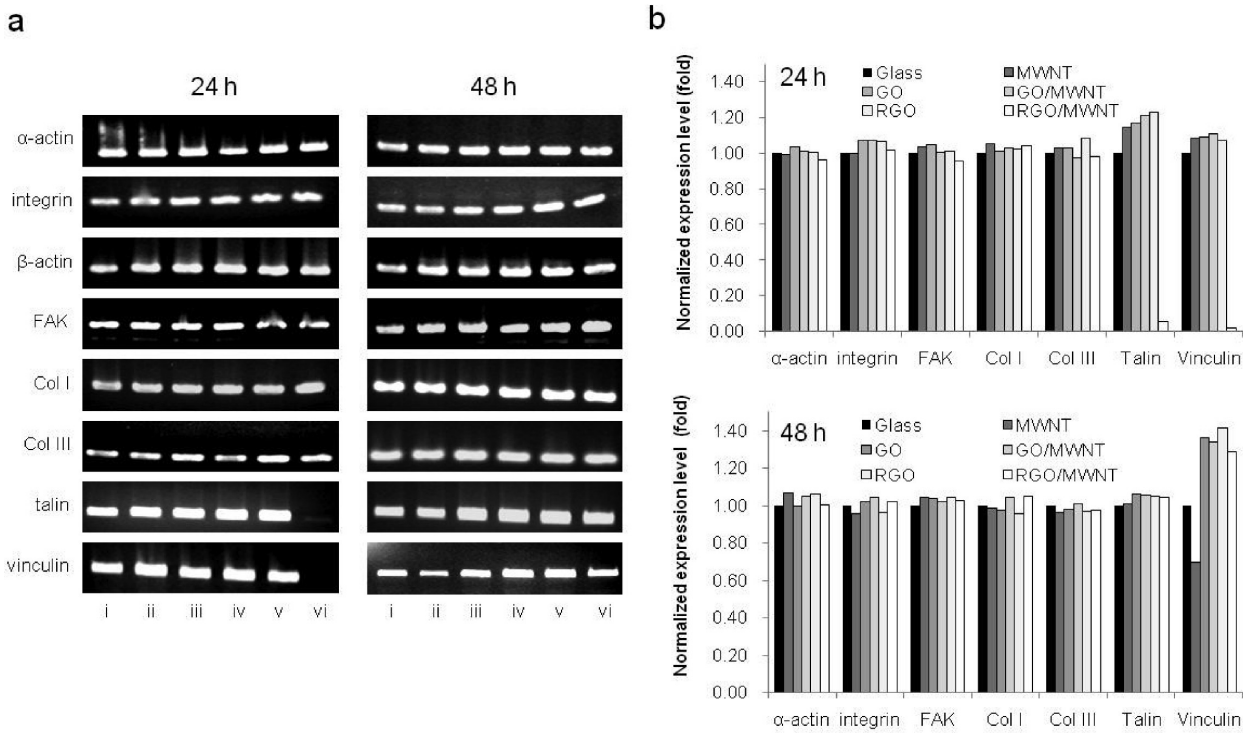

Figure 6. Expression profiles of cell adhesion- and cell spreading-associated genes. Agarose gel (1.5%) electrophoresis of RT-PCR products of cell adhesion-associated genes of cells cultured on (i) glass; (ii) MWNT; (iii) GO; (iv) GO/MWNT; (v) RGO; and (vi) RGO/MWNT substrates (a). Expression levels of adhesion-associated genes normalized to those of control cells (100%) (b). PCR products were quantitated using TINA 2.0 software (Raytest, Straubenhardt, Germany).

expression formed smaller focal contacts, localized all over the ventral face, and displayed a marked decrease in the number of stress fibers.[43] It is intriguing to note that, in our study, the number of focal adhesions remained similar, regardless of changes in the expression of talin and vinculin. This phenomenon warrants further study.

To demonstrate the usefulness of carbon-based nanomaterial-coated substrates in biological studies, we performed gene transfection studies on cells grown on these substrates (Figure 7). Hydrophobic culture substrates are known to enhance gene transfection efficiency,[44] and thus we expected that the coated substrates would enhance gene transfection efficiency. To investigate the gene transfection efficiency, we transfected NIH-3T3 cells grown on the different substrates with a plasmid encoding green fluorescent protein (GFP), using Lipofectamine 2000 as a transfection agent, at a ratio of 1 μg of pGFP to 1 μL of Lipofectamine 2000, and cells seeded at a density of 20−26% (6×10^4 cells per well in 12-well cell culture plates). GFP expression was observed by both fluorescence microscopy and flow cytometry (Figure 7). Cells grown on the modified substrates showed higher GFP expression, as expected. Cells cultured on the GO- and RGO-coated substrates showed greatly enhanced GFP fluorescence, up to a 250% increase compared with cells on bare glass. Interestingly, cells seeded at higher density, 70−80%, gave no significant difference in GFP expression among the substrates (data not shown). It seems that sparsely distributed cells tend to be more sensitive to substrate properties.

Encouraged by the enhanced transfection efficiency of NIH-3T3 cells, we performed gene transfection experiments using HeLa cells, a cervical cancer cell line, under the conditions described above. The HeLa cells showed enhanced GFP expression of up to 200%, with the highest expression observed on the RGO/MWNT surface after 24 h of incubation (Figure 7). On the basis of our work, it appears that gene transfection may be enhanced, at least to some degree, for some cell types by culturing the cells on the carbon nanomaterial-coated substrates.

To evaluate the effect of surface properties, the gene transfection efficiencies were plotted with contact angles and surface roughness (Figure 8). The contact angles of the modified substrates are considered as moderately wettable substrates (not too hydrophobic) with values less than 90°. The transfection efficiency of NIH-3T3 and HeLa cells at 48 h post-transfection was increased on the carbon nanomaterial-coated substrates, which have relatively high contact angle values compared with sterile glass (Figure 8a,c). On the other hand, the transfection efficiency was enhanced on the relatively less rough substrates, GO, GO/MWNT, RGO, and RGO/MWNT, both in NIH-3T3 and HeLa cells (Figure 8b,d). However, NIH-3T3 cells showed more dramatic increase than HeLa cells in the gene transfection efficiency on the less rough substrates at 48 h post-

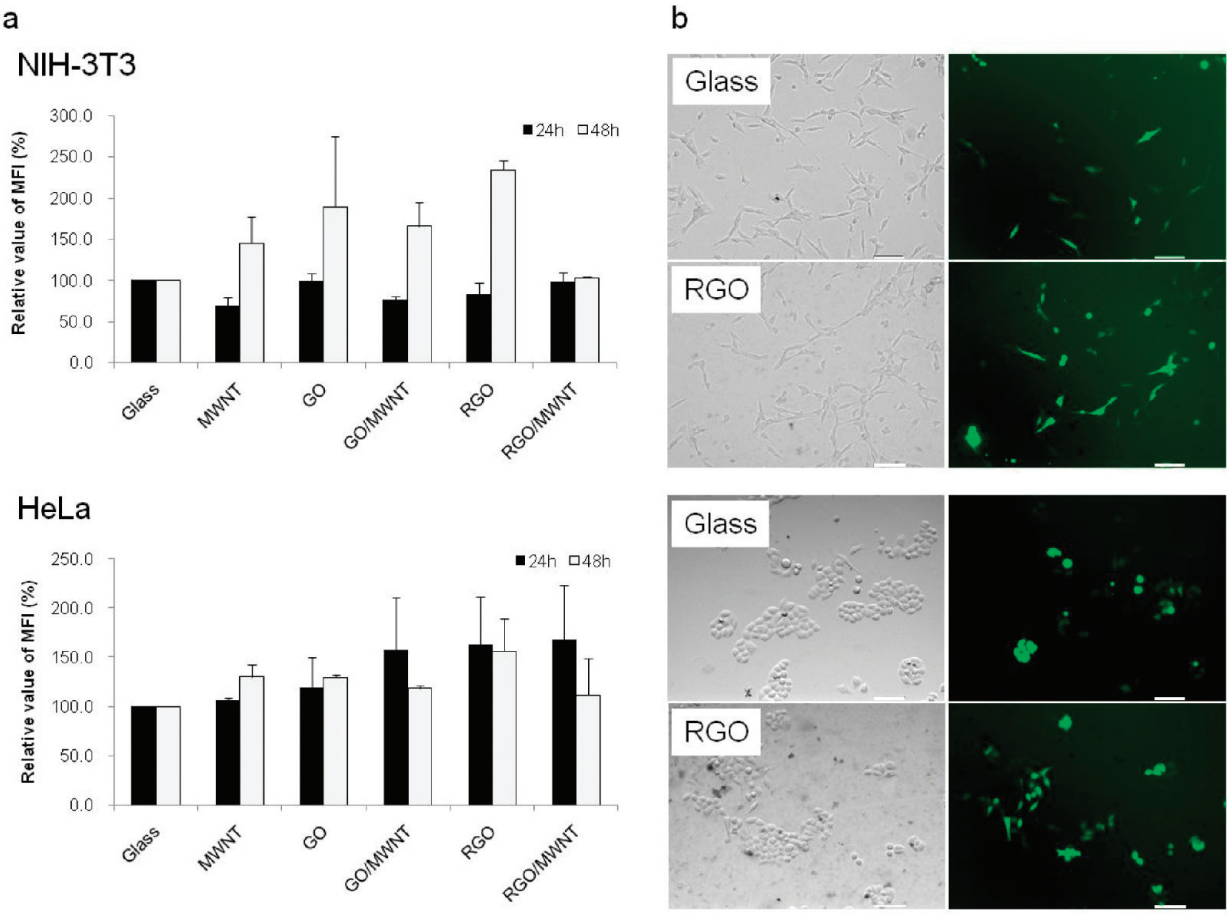

Figure 7. Gene transfection efficiency of NIH-3T3 and HeLa cells cultured for 24 and 48 h on the indicated substrates. The cells were transfected with 1 μg of pGFP, encoding green fluorescent protein, using a transfection reagent, Lipofectamine 2000. At 24 and 48 h post-transfection, the transfection efficiency was assessed *via* flow cytometry. Data are presented as the percentage mean fluorescence intensity (MFI) ± standard error mean (SEM). Representative images of pGFP-transfected cells (top, NIH-3T3 on RGO; bottom, HeLa on RGO) after 48 h incubation on the substrate were shown in (b). Scale bars: 35 μm.

transfection. It seemed that the differences were attributed to the distinctive properties of each cell line.

CONCLUSIONS

In summary, we characterized five carbon-based nanomaterial-coated substrates (MWNT, GO, GO/MWNT, RGO, and RGO/MWNT) with respect to biocompatibility and cell behavior, focusing on cell adhesion, proliferation, spreading, focal adhesion, and gene transfection efficiency. Given that the carbon-based nanomaterials used in the present study are being incorporated into systems that may come into contact with cells, both *in vivo* (*i.e.*, coatings for implantable devices and cell-based sensors) and *in vitro*, it is of great importance to study cell behavior, survival, and function on the substrates. The present study makes several contributions to these efforts. First, we developed substrates to which carbon-based materials, including graphene and MWNTs, are attached *via* covalent conjugation. Many biological applications require sturdy coatings that remain intact for long periods of time to prevent undesirable side effects from exfoliated nanomaterials (see Figure S5 in Supporting Information for intact nanomaterial coating after cell culture and cell detachment by trypsin treatment). Second, we show, through a systematic series of experiments, that these substrates may be readily used for cell-interfacing systems and are compatible with biosystems. Thorough investigations of cellular behaviors, as in the present study, can help to establish a set of standard assays for judging biocompatibility and cell-friendliness of nanomaterial-coated surfaces. Third, these modified substrates are useful for the gene transfection of cells at low cell densities. In our experience, mammalian cells cultured at low density appear to experience greater toxicity upon exposure to transfection agents, making it difficult to achieve high levels of gene transfection. The substrates coated with GO, RGO, and/or MWNTs can provide favorable environments for transfection, although the detailed mechanism is currently unknown.

The present study provides quantitative information on biocompatibility of supported thin films of graphene/MWNT, the cell behaviors depending on the substrate properties and the improvement in gene transfection efficiencies of mammalian cells grown on

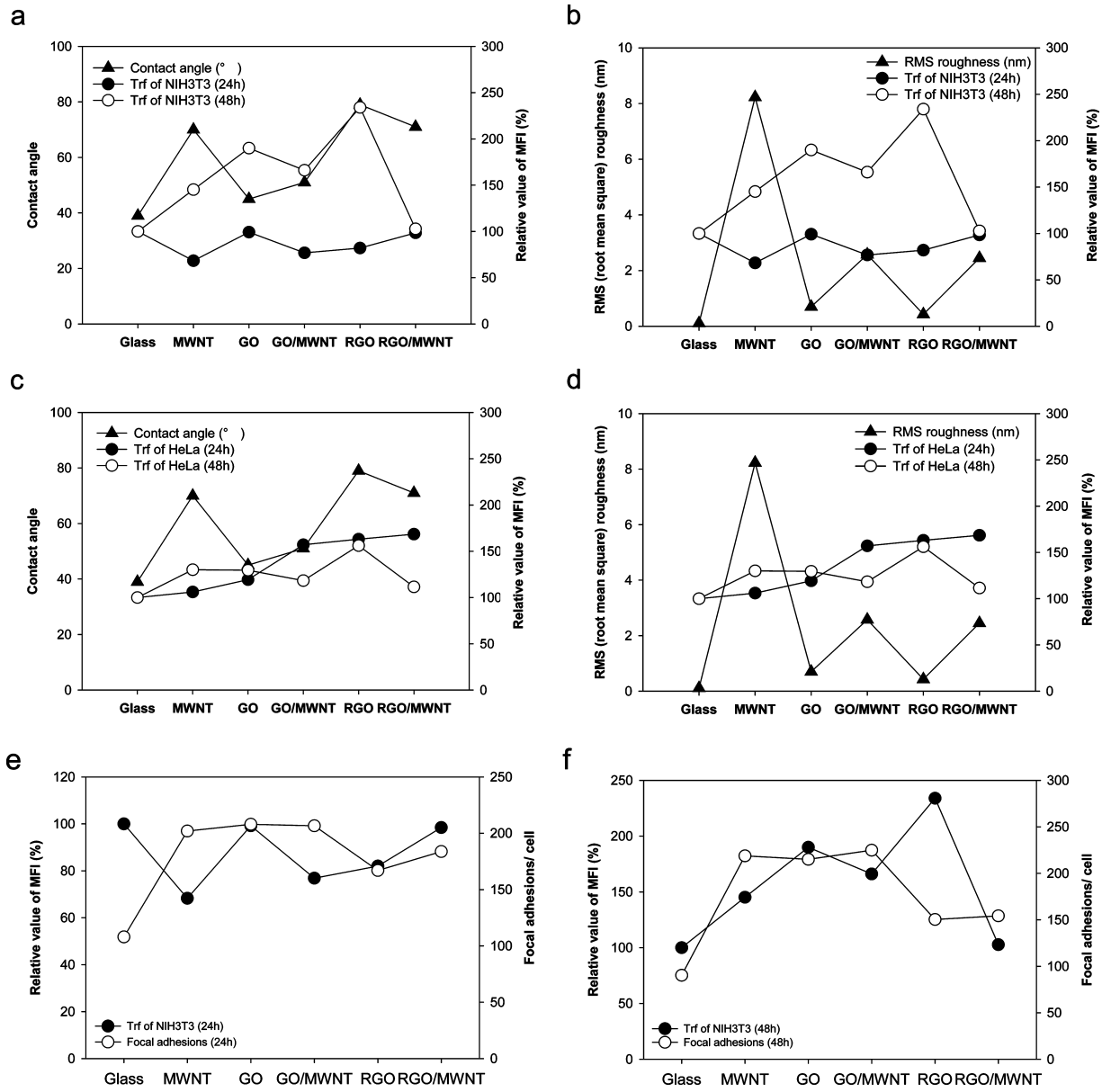

Figure 8. Relationship of contact angle (a,c), surface roughness (b,d), and focal adhesion numbers (e,f) of carbon nanomaterial-coated substrate with gene transfection efficiencies. The cells were cultured on various types of substrates coated with carbon nanomaterials for 24 and 48 h, and sterile glass was used as control substrate (for NIH-3T3 (a,b,e,f) and for HeLa (c,d)).

those substrates. We are certain that the present study has enhanced our understanding of cellular responses and behaviors at the interface between mammalian cells and carbon-based nanomaterials. The study suggests that these nanomaterials hold high potential for bioapplications showing high biocompatibility, especially as surface coating materials for implants, without inducing notable deleterious effects.

METHODS

Materials. Graphite oxide was prepared from natural graphite (FP 99.95%pure, Graphit Kropfmuhl AG (Hauzenberg, Germany) using Hummer's method. The synthesized graphite oxide was suspended in water by brief sonication. The suspension was centrifuged at 8000 rpm for 10 min, and the supernatant was used for the following experiment. MWNTs produced by chemical vapor deposition (95% pure, length 5−20 μm, outer diameter 15 ± 5 nm) were purchased from NANOLAB (Massachusetts, USA). Hydrogen peroxide (30% in water) and sodium nitrate were purchased from Junsei (Japan). Potassium permanganate, ethylene diamine, anhydrous dimethylformamide (DMF), anhydrous toluene, 3-glycidoxypropyltrimethoxysilane (3-GPTMS), and 3-aminopropyltriethoxysilane (3-APTES) were purchased from Sigma-Aldrich (St. Louis, MO). Sulfuric acid and nitric acid were purchased from Samchun (Seoul, Korea). Ethanol was purchased from Merck (Darmstadt, Germany). Glass coverslips (#2, 0.19 to 0.23 mm in thickness) were purchased from VWR (West Chester, USA). All chemicals were used without further purification.

Preparation of Substrates Coated with Films of Graphene and/or MWNTs. Glass substrates were cleaned by immersing into piranha solution (hydrogen peroxide (30%)/sulfuric acid = 1:3; WARNING! Piranha solution is highly dangerous; handle with caution) for 10

min at 120 °C, washed with water and ethanol, and dried by blowing nitrogen gas. The cleaned substrates were immersed in 10 mM anhydrous toluene solution of 3-APTES for 30 min, briefly sonicated in toluene, washed with ethanol and water, dried by blowing nitrogen gas, and baked at 125 °C under nitrogen stream. Graphene oxide sheets were immobilized on the 3-APTES-treated substrate *via* electrostatic interaction by immersing the substrates in graphene oxide aqueous suspension (1.5 mg/mL) for 1 h, washed with water and ethanol, and dried by blowing nitrogen gas. This graphene-coated substrate was immersed in an aqueous suspension of aminated MWNTs (120 μg/mL) for 1 h, washed with water and ethanol, and dried under a stream of nitrogen gas. The graphene oxide and/or MWNT-coated substrates were chemically reduced by immersing into 20% DMF solution of hydrazine monohydrate for a day at 80 °C, washed with DMF, water, and ethanol, and dried under a stream of nitrogen gas. Prior to being employed as a cell culture substrate or chemical reduction, graphene oxide and/or MWNT-coated substrates were baked at 125 °C under nitrogen stream. For preparation of MWNT-coated glass substrates, the piranha-treated substrates were immersed in 10 mM anhydrous toluene solution of 3-GPTMS for 30 min, washed with toluene, ethanol, and water, and dried by blowing nitrogen gas. The 3-GPTMS-treated substrates were immersed in an aqueous suspension of aminated MWNT (120 μg/mL) for 1 h, washed with water and ethanol, dried by blowing nitrogen gas, and baked at 125 °C under nitrogen stream.

Characterization of the Substrates. The atomic force microscopy image and profile of exfoliated graphene oxide sheets were taken with an XE-100 (Park system) using a backside gold-coated silicon probe (M to N, Korea). FT-IR spectra measurements of graphite and graphite oxide were carried out with an EQUINOX55 (Bruker, Germany) by the KBr pellet method. The surface morphology of five different graphene and/or MWNT-coated substrates was observed by S-4800 field emission scanning electron microscopy (Hitach, Japan). The UV−vis spectra of the graphene and/or MWNT thin films on substrates were obtained with a UV-2550 (Shimadzu, Japan). Raman analysis of the graphene and/or MWNT-coated substrates was conducted by LabRAM HR UV/vis/NIR (Horiba jobin Yvon, France) using an Ar ion CW laser (514.5 nm) as an excitation source focused through a BXFM confocal microscope with an objective lens (50×, numerical aperture = 0.50). High-resolution XPS measurements were performed with an ESCA 2000 (Thermo VG Science, USA) with twin X-ray source (Mg/Al target). Water contact angle measurements were performed by Phoenix300 (S.E.O., Korea).

Cell Culture. NIH-3T3 (mouse embryonic fibroblast cell line) cells were cultured in Dulbecco's modified Eagle's medium (DMEM) containing 4.5 g/L D-glucose and supplemented with 10% FBS (fetal bovine serum), 100 units/mL penicillin, and 100 μg/mL streptomycin at 37 °C at 5% CO_2. NIH-3T3 cells were seeded on the substrate modified with GO and MWNT, where $1-2 \times 10^5$ cells were plated per substrate (about 30−50% confluency for the experiments unless otherwise indicated). After incubation either for 24 or 48 h and brief washing with sterilized PBS, images of NIH-3T3 cells on the substrate were observed.

Immunostaining. NIH-3T3 cells were seeded on each experimental substrate and cultured at 37 °C in the presence of serum. Cells were washed with PBS and fixed in 4% paraformaldehyde in PBS (pH 7.4) for 20 min at room temperature. After fixation, cells were washed with PBS and then treated with 0.1% Triton X-100 in PBS for 5 min and blocking solution (1% BSA in PBS) for 30 min. To visualize focal adhesions, cells were treated with antivinculin antibody (Sigma, St. Louis, MO) diluted 1:400 in blocking solution for 1 h, followed by incubation with goat anti-mouse Alexa Fluor 488 antibody (Molecular Probes, Eugene, OR) at 1:400 dilution in blocking buffer for 1 h. For double labeling, TRITC-conjugated phalloidin was incubated simultaneously with the secondary antibody. Slides were washed three times with PBS between each antibody treatment.

Biocompatibility Test. The biocompatibility of carbon-based nanomaterials immobilized on the substrate was tested by examining the growth of NIH-3T3 cells using the live/dead viability/cytotoxicity assay kit (Molecular Probes Invitrogen). NIH-3T3 cells were seeded at 6×10^5 cells per well of a 6-well cell culture plate. The cells were incubated on each substrate for 24 and 48 h. Following incubation, 50 μL of the combined live/dead cell staining solution (2 μM calcein AM and 4 μM EthD-1 in D-PBS) was added to each substrate and incubated with cells for 30−45 min at room temperature. Images were obtained using a BX51M optical microscope (Olympus Co., Japan) equipped with fluorescence light source and filters.

Cell Proliferation Assay. The NIH-3T3 cells were seeded on the substrate immobilized with various carbon-based nanomaterials for 24 and 48 h, and then the cells were stained with the live/dead viability/cytotoxicity assay kit (from Molecular Probes Invitrogen). The number of live cells were counted and analyzed by using NIH ImageJ, and data represent mean ± SEM of at least three different images.

Image Analysis. Images were collected using a Ti inverted fluorescence microscope equipped with a 60× (1.4 numerical aperture) objective (Nikon Co., Japan) and a CoolSNAPcf charge-coupled device (CCD) camera (Photometrics, Tucson, AZ) with Metamorph image analysis software (Molecular Devices, Sunnyvale, CA). Cell areas were quantified using the ImageJ software package (NIH) to trace cell cytoplasmic borders. Focal adhesions were visualized by indirect immunofluorescence using an antivinculin antibody. Focal adhesion area and number per cell were determined using NIH ImageJ software. The nuclear space index (NSI) was calculated as maximal nuclear area in the $x-y$ plane divided by nuclear height. The measurement of cell shape index (CSI) or roundness values for each cellular contour, with 1 representing a perfect circle and 0 a straight line, was based on the ratio of cell width to cell length.

RT-PCR. NIH-3T3 cells were cultured on each substrate and incubated either for 24 or 48 h; sterile glass was used as control substrate. Total RNA was extracted by using Trizol reagent (Invitrogen) according to the manufacturer's instructions. Total RNA was quantified, and the quality of total RNA was analyzed based on the 28S:18S rRNA ratio by using agarose gel electrophoresis. Total RNA samples (2 mg each) were used for reverse transcription under standard conditions (SuperScript II reverse transcriptase; Invitrogen). The resulting cDNA was used as template in subsequent PCR amplifications. Sequences of interest were amplified by using the following primer pairs: α-actin (5′-ATCTGGCACCACACCTTCTA-3′/5′-AGCTCGTAGCTCTTCTCCAG-3′), integrin (5′-GACCTGCCTTGGTGTCTGTGC-3′/5′-AGCAACCACACCAGCTACAAT-3′), FAK (5′-GTAGTGAGCCAACCACCTGG-3′/5′- GCCCTTGTCTGTCAGGTAAC-3′), type I collagen (5′-ACTGGTACATCAGCCCGAAC-3′/5′-GGTGGAGGGAGTTTACACGA-3′), type III collagen (5′-GCTGGCATTCCTCAG ACTTC-3′/5′- TAGTCTCATTGCCTTGCGTG-3′), talin (5′-GAAATTGAGGCCAAGGTCCG-3′/5′-GCCTTCAGTCGTCTGTACTG-3′), and vinculin (5′-AGCAGGAGTTGACTCACCAG-3′/5′-TCTAAGATCTGCCTGATGGC-3′). β-Actin (5′-GCTCGTCGTCGACAACGGCTC-3′/5′-CAAACATGATCTGGGTCATCTTCTT-3′) was used as endogenous reference housekeeping gene. The PCR reactions for α-actin, β-actin, and integrin were performed as follows: 5 min at 94 °C (30 s at 94 °C, 30 s at 58 °C, 30 s at 72 °C) × 35 cycles, 5 min at 72 °C. The PCR reaction for FAK was performed as follows: 5 min at 94 °C (2 min at 94 °C, 30 s at 60 °C, 1 min at 72 °C) × 35 cycles, 5 min at 72 °C. The conditions of PCR reactions for Col I and Col III were performed as follows: 5 min at 94 °C (30 s at 94 °C, 30 s at 54 °C, 30 s at 72 °C) × 35 cycles. The conditions of PCR reactions for talin and vinculin were as follows: 5 min at 94 °C (2 min at 94 °C, 30 s at 54 °C, 1 min at 72 °C) × 35 cycles. Relative intensity of each mRNA level bands normalized to β-actin was quantified using the Tina 2.0 software (Raytest, Straubenhardt, Germany).

Gene Transfection. NIH-3T3 mouse fibroblast and HeLa cells were seeded on each substrate in 12-well cell culture plates at 6×10^4 cells per well. The cells were grown in an incubator at 37 °C and 5% CO_2. The NIH-3T3 cells were transfected with the GFP expressing plasmid (pGFP) in serum-free media using Lipofectamine 2000 (Invitrogen) according to the manufacturer's protocol. After 4 h incubation with1 μg of pDNA in lipoplexes, cells were returned to culture with a medium containing 10% FBS (fetal bovine serum), 100 units/mL penicillin, and 100 μg/mL streptomycin and grown at 37 °C and 5% CO_2 until the transfec-

tion efficiency was measured. The fluorescence intensity of positive cells was measured with a flow cytofluorometer (Becton Dickinson, USA) equipped with an argon laser.

Acknowledgment. This work was supported by Basic Science Research Program through the National Research Foundation of Korea (NRF) funded by the Korean government (MEST) (Grant Nos. 313-2008-2-C00538, 2008-0062074), by the Nano R&D program of NRF funded by MEST (2008-2004457), and by the National Honor Scientist Program of the Ministry of Education, Science and Technology in Korea.

Supporting Information Available: Analytical data. This material is available free of charge *via* the Internet at http://pubs.acs.org.

REFERENCES AND NOTES

1. Yang, H.; Xia, Y. Bionanotechnology: Enabling Biomedical Research with Nanomaterials. *Adv. Mater.* **2007**, *19*, 3085–3087.
2. Yang, W.; Ratinac, K. R.; Ringer, S. P.; Thordarson, P.; Gooding, J. J.; Braet, F. Carbon Nanomaterials in Biosensors: Should You Use Nanotubes or Graphene? *Angew. Chem., Int. Ed.* **2010**, *49*, 2114–2138.
3. Chen, H.; Jiang, C.; Yu, C.; Zhang, S.; Liu, B.; Kong, J. Protein Chips and Nanomaterials for Application in Tumor Marker Immunoassays. *Biosens. Bioelectron.* **2009**, *24*, 3399–3411.
4. Xia, Y. Nanomaterials at Work in Biomedical Research. *Nat. Mater.* **2008**, *7*, 758–760.
5. Liu, H.; Webster, T. J. Nanomedicine for Implants: A Review of Studies and Necessary Experimental Tools. *Biomaterials* **2007**, *28*, 354–369.
6. Kim, J.; Kim, H. S.; Lee, N.; Kim, T.; Kim, H.; Yu, T.; Song, I. C.; Moon, W. K.; Hyeon, T. Multifunctional Uniform Nanoparticles Composed of a Magnetite Nanocrystal Core and a Mesoporous Silica Shell for Magnetic Resonance and Fluorescence Imaging and for Drug Delivery. *Angew. Chem., Int. Ed.* **2008**, *47*, 8438–8441.
7. Kim, J.; Piao, Y.; Hyeon, T. Multifunctional Nanostructured Materials for Multimodal Imaging, and Simultaneous Imaging and Therapy. *Chem. Soc. Rev.* **2009**, *38*, 372–390.
8. Dikin, D. A.; Stankovich, S.; Zimney, E. J.; Piner, R. D.; Dommett, G. H. B.; Evmenenko, G.; Nguyen, S. T.; Ruoff, R. S. Preparation and Characterization of Graphene Oxide Paper. *Nature* **2007**, *448*, 457–460.
9. Berger, C.; Song, Z.; Li, T.; Li, X.; Ogbazghi, A. Y.; Feng, R.; Dai, Z.; Marchenkov, A. N.; Conrad, E. H.; First, P. N.; *et al.* Ultrathin Epitaxial Graphite: 2D Electron Gas Properties and a Route toward Graphene-Based Nanoelectronics. *J. Phys. Chem. B* **2004**, *108*, 19912–19916.
10. Trauzettel, B.; Bulaev, D. V.; Loss, D.; Burkard, G. Spin Qubits in Graphene Quantum Dots. *Nat. Phys.* **2007**, *3*, 192–196.
11. Kim, K. S.; Zhao, Y.; Jang, H.; Lee, S. Y.; Kim, J. M.; Kim, K. S.; Ahn, J.-H.; Kim, P.; Choi, J. Y.; Hong, B. H. Large-Scale Pattern Growth of Graphene Films for Stretchable Transparent Electrodes. *Nature* **2009**, *457*, 706–710.
12. Wang, D.; Kou, R.; Choi, D.; Yang, Z.; Nie, Z.; Li, J.; Saraf, L. V.; Hu, D.; Zhang, J.; Graff, G. L.; *et al.* Ternary Self-Assembly of Ordered Metal Oxide-Graphene Nanocomposites for Electrochemical Energy Storage. *ACS Nano* **2010**, *4*, 1587–1595.
13. Harrison, B. S.; Atala, A. Carbon Nanotube Applications for Tissue Engineering. *Biomaterials* **2007**, *28*, 344–353.
14. Kaya, C.; Singh, I.; Boccaccini, A. R. Multi-walled Carbon Nanotube-Reinforced Hydroxyapatite Layers on Ti_6Al_4V Medical Implants by Electrophoretic Deposition (EPD). *Adv. Eng. Mater.* **2008**, *10*, 131–138.
15. He, S.; Song, B.; Li, D.; Zhu, C.; Qi, W.; Wen, Y.; Wang, L.; Song, S.; Fang, H.; Fan, C. A Graphene Nanoprobe for Rapid, Sensitive, and Multicolor Fluorescent DNA Analysis. *Adv. Funct. Mater.* **2010**, *20*, 453–459.
16. Jang, H; Kim, Y. K.; Kwon, H. M.; Yeo, W. S.; Kim, D. E.; Min, D. H. A Graphene-Based Platform for the Assay of Duplex-DNA Unwinding by Helicase. *Angew. Chem., Int. Ed.* **2010**, *49*, 5703–5707.
17. De La Zerda, A.; Zavaleta, C.; Keren, S.; Vaithilingam, S.; Bodapati, S.; Liu, Z.; Levi, J.; Smith, B. R.; Ma, T. J.; Oralkan, O.; *et al.* Carbon Nanotubes as Photoacoustic Molecular Imaging Agents in Living Mice. *Nat. Nanotechnol.* **2008**, *3*, 557–562.
18. Liu, Z.; Robinson, J. T.; Sun, X.; Dai, H. PEGylated Nanographene Oxide for Delivery of Water-Insoluble Cancer Drugs. *J. Am. Chem. Soc.* **2008**, *130*, 10876–10877.
19. Hu, W.; Peng, C.; Luo, W.; Lv, M.; Li, X.; Li, D.; Huang, Q.; Fan, C. Graphene-Based Antibacterial Paper. *ACS Nano* **2010**, *4*, 4317–4323.
20. Aplin, A. E.; Howe, A. K.; Juliano, R. L. Cell Adhesion Molecules, Signal Transduction and Cell Growth. *Curr. Opin. Cell Biol.* **1999**, *11*, 737–744.
21. Shin, Y. M.; Kim, K. S.; Lim, Y. M.; Nho, Y. C.; Shin, H. Modulation of Spreading, Proliferation, and Differentiation of Human Mesenchymal Stem Cells on Gelatin-Immobilized Poly(L-lactide-*co*-caprolactone) Substrates. *Biomacromolecules* **2008**, *9*, 1772–1781.
22. Kong, H. J.; Liu, J. D.; Riddle, K.; Matsumoto, T.; Leach, K.; Mooney, D. J. Non-viral Gene Delivery Regulated by Stiffness of Cell Adhesion Substrates. *Nat. Mater.* **2005**, *4*, 460–464.
23. Discher, D. E.; Janmey, P.; Wang, Y. L. Tissue Cells Feel and Respond to the Stiffness of Their Substrate. *Science* **2005**, *310*, 1139–1143.
24. Huang, J.; Gräter, S. V.; Corbellini, F.; Rinck, S.; Bock, E.; Kemkemer, R.; Kessler, H.; Ding, J.; Spatz, J. P. Impact of Order and Disorder in RGD Nanopatterns on Cell Adhesion. *Nano Lett.* **2009**, *9*, 1111–1116.
25. Oh, S.; Brammer, K. S.; Li, Y. S.; Teng, D.; Engler, A. J.; Chien, S.; Jin, S. Stem Cell Fate Dictated Solely by Altered Nanotube Dimension. *Proc. Natl. Acad. Sci. U.S.A.* **2009**, *106*, 2130–2135.
26. Brunetti, V.; Maiorano, G.; Rizzello, L.; Sorce, B.; Sabella, S.; Cingolani, R.; Pompa, P. P. Neurons Sense Nanoscale Roughness with Nanometer Sensitivity. *Proc. Natl. Acad. Sci. U.S.A.* **2010**, *107*, 6264–6269.
27. Gallant, N. D.; Capadona, J. R.; Frazier, A. B.; Collard, D. M.; García, A. J. Micropatterned Surfaces To Engineer Focal Adhesions for Analysis of Cell Adhesion Strengthening. *Langmuir* **2002**, *18*, 5579–5584.
28. Fletcher, D. A.; Mullins, R. D. Cell Mechanics and the Cytoskeleton. *Nature* **2010**, *463*, 485–492.
29. Malarkey, E. B.; Fisher, K. A.; Bekyarova, E.; Liu, W.; Haddon, R. C.; Parpura, V. Conductive Single-Walled Carbon Nanotube Substrates Modulate Neuronal Growth. *Nano Lett.* **2009**, *9*, 264–268.
30. Kim, Y. K.; Min, D. H. Durable Large-Area Thin Films of Graphene/Carbon Nanotube Double Layers as a Transparent Electrode. *Langmuir* **2009**, *25*, 11302–11306.
31. Ponsonnet, L.; Reybier, K.; Jaffrezic, N.; Comte, V.; Lagneau, C.; Lissac, M.; Martelet, C. Relationship between Surface Properties (Roughness, Wettability) of Titanium and Titanium Alloys and Cell Behaviour. *Mater. Sci. Eng., C* **2003**, *23*, 551–560.
32. Humphries, J. D.; Wang, P.; Streuli, C.; Geiger, B.; Humphries, M. J.; Ballestrem, C. Vinculin Controls Focal Adhesion Formation by Direct Interactions with Talin and Actin. *J. Cell Biol.* **2007**, *179*, 1043–1057.
33. Thakar, R. G.; Cheng, Q.; Patel, S.; Chu, J.; Nasir, M.; Liepmann, D.; Komvopoulos, K.; Li, S. Cell-Shape Regulation of Smooth Muscle Cell Proliferation. *Biophys. J.* **2009**, *96*, 3423–3432.
34. Thomas, C. H.; Collier, J. H.; Sfeir, C. S.; Healy, K. E. Engineering Gene Expression and Protein Synthesis by Modulation of Nuclear Shape. *Proc. Natl. Acad. Sci. U.S.A.* **2002**, *99*, 1972–1977.
35. Schwartz, M. A.; Ginsberg, M. H. Networks and Crosstalk: Integrin Signalling Spreads. *Nat. Cell Biol.* **2002**, *4*, E65–E68.
36. Chen, C. S.; Alonso, J. L.; Ostuni, E.; Whitesides, G. M.;

Ingber, D. E. Cell Shape Provides Global Control of Focal Adhesion Assembly. *Biochem. Biophys. Res.Commun.* **2003**, *307*, 355–361.
37. Kato, M.; Mrksich, M. Using Model Substrates To Study the Dependence of Focal Adhesion Formation on the Affinity of Integrin-Ligand Complexes. *Biochemistry* **2004**, *43*, 2699–2707.
38. Hood, J. D.; Cheresh, D. A. Role of Integrins in Cell Invasion and Migration. *Nat. Rev. Cancer* **2002**, *2*, 91–100.
39. Mitra, S. K.; Hanson, D. A.; Schlaepfer, D. D. Focal Adhesion Kinase: In Command and Control of Cell Motility. *Nat. Rev. Mol. Cell Biol.* **2005**, *6*, 56–68.
40. Galbraith, C. G.; Yamada, K. M.; Sheetz, M. P. The Relationship between Force and Focal Complex Development. *J. Cell Biol.* **2002**, *159*, 695–705.
41. Bendori, R.; Salomon, D.; Geiger, B. Contact-Dependent Regulation of Vinculin Expression in Cultured Fibroblasts: A Study with Vinculin-Specific cDNA Probes. *EMBO J.* **1987**, *6*, 2897–2905.
42. Ungar, F.; Geiger, B.; Ben-Ze'ev, A. Cell Contact- and Shape-Dependent Regulation of Vinculin Synthesis in Cultured Fibroblasts. *Nature* **1986**, *319*, 787–791.
43. Albiges-Rizo, C.; Frachet, P.; Block, M. R. Down Regulation of Talin Alters Cell Adhesion and the Processing of the Alpha 5 beta 1 Integrin. *J. Cell Sci.* **1995**, *108*, 3317–3329.
44. Shiu, J. Y.; Kuo, C. W.; Whang, W. T.; Chen, P. Observation of Enhanced Cell Adhesion and Transfection Efficiency on Superhydrophobic Surfaces. *Lab Chip* **2010**, *10*, 556–558.